ACS APPLIED MATERIALS & INTERFACES

Research Article

www.acsami.org

Study on Thermal Evolution of the CuSe Phase in Nanoparticle-Based Absorber Layers for Solution-Processed Chalcopyrite Photovoltaic Devices

Yeong-Hui Seo,[†] Byung-Seok Lee,[‡] Yejin Jo,[†] Han-Gyeol Kim,[†] Kyoohee Woo,[§] Jooho Moon,[§] Youngmin Choi,[†] Beyong-Hwan Ryu,[†] and Sunho Jeong*[,†]

[†]Advanced Materials Division, Korea Research Institute of Chemical Technology (KRICT), 141 Gajeongro, Yuseong, Daejeon 305-600, Korea

[‡]Advanced Materials Lab, Global Technology, SK Innovation, 325, Exporo, Yuseong, Daejeon, 325-712, Korea

[§]Department of Materials Science and Engineering, Yonsei University, 50 Yonsei-ro, Seodaemun-gu, Seoul, 120-749, Korea

Supporting Information

ABSTRACT: Nanoparticle-based, solution-processed chalcopyrite photovoltaic devices have drawn tremendous attraction for the realization of low-cost, large-area solar cell applications. In particular, it has been recently demonstrated that the CuSe phase plays a critical role in allowing the formation of device-quality, nanoparticle-based chalcopyrite absorber layers. For further in-depth study, with the aim of understanding the thermal behavior of the CuSe phase that triggers the vigorous densification reaction, a requisite for high-performance chalcopyrite absorber layers, both multiphase (CuSe-phase including) and single-phase (CuSe-phase free) CISe nanoparticles are investigated from the viewpoint of compositional variation and crystalline structural evolution. In addition, with CuSe-phase including CISe particulate layers, the basic restrictions in thermal treatment necessary for activating effectively the CuSe-phase induced densification reaction are suggested, in conjunction with consideration on the thermal decomposition of organic additives that are inevitably incorporated in nanoparticle-based absorber layers.

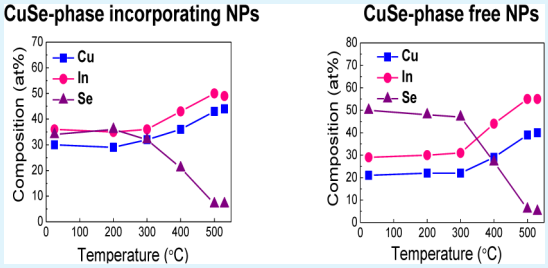

KEYWORDS: *CuSe, nanoparticle, absorber, solution-processed, chalcopyrite, photovoltaic device*

1. INTRODUCTION

Chalcopyrite compounds, $Cu(In,Ga)(S,Se)_2$, have been regarded as promising light absorbers in photovoltaic device applications owing to their high absorption coefficient and also to their band gap, which is adjustable depending on the In/Ga and S/Se ratios.[1] Device-quality absorber layers have been, in general, created by depositing each element in the form of vapor phase through either evaporation or sputtering techniques.[2] However, the high manufacturing cost poses an inhibitory in realizing large-area, low cost, high performance photovoltaic devices. In contrast, the solution-processed deposition techniques, based on the soluble functional materials, could allow a variety of advantages, including a less energy intensive route, scalability, simplicity, and high throughput, over conventional vacuum-deposition methods.

However, nanoparticle-based, solution-processable materials have been shown to have limitations in improving device performance due to the inherent nature of chalcopyrite-phase nanoparticles.[3] In order to establish an electrical path for efficient charge carrier conduction, a well-interconnected, dense particulate structure should be evolved during annealing at elevated temperatures, generally below 550 °C. However, by annealing in such a temperature region, no interparticular junction between neighboring nanoparticles is generated, which gives rise to restrictions in accomplishing high-performance photovoltaic devices. In this regard, in spite of their easy accessibility on large-area, low-cost solar cell applications, nanoparticle-based chemical pathways have been reported only in a limited number of studies due to the lack of strategies for provoking the chemical activation for densification reactions; on the other hand, with precursor-solution based techniques, facile methodologies have been demonstrated for creating dense, solution-processed chalcopyrite absorber layers.[4]

Recently, in nanoparticle-based approaches, two specific methodologies have opened the novel possibility of enabling highly efficient devices: (i) densification through elemental substitution between S and Se element[4,5] and (ii) liquid-phase densification triggered by the low melting-point phase, CuSe, which is transformed into the desired chalcopyrite phase during annealing at elevated temperatures.[6,7] In particular, the latter case possesses the versatility to allow it to be applied to various material systems. Furthermore, the physical/chemical mecha-

Received: February 7, 2013
Accepted: June 21, 2013
Published: June 21, 2013

   dx.doi.org/10.1021/am401735a | ACS Appl. Mater. Interfaces 2013, 5, 6930−6936

nisms of the CuSe phase for densification reactions have been clarified in impurity-free chalcopyrite absorber layers. There have been several theoretical reports on the transition of CuSe binary phases formed by a sequential evaporation,[8] sputtering,[9−11] chemical bath deposition,[12,13] and chemical vapor deposition.[14] Studies of CuSe binary phase transitions, however, have rarely been reported for nanoparticle-based thin-films, even if the CuSe nanoparticles have been synthesized by various chemical approaches.[15−18] The realization of CuSe-phase induced densification reaction has not been achieved due to the chemical/thermal instability of CuSe phase in solution-processed films, even if the CuSe phase has been well-manipulated for adjusting the microstructural quality in vacuum-deposited CI(G)S films. In nanoparticle-based thin-films, the organic components should be incorporated in films as both a capping molecule (to stabilize the nanoparticle surface) and an organic additive (to meet the rheological requirements adequate for the wet-coating method), which alters the kinetic activity in phase transitions. In addition, the annealing processes in air should be involved in order to effectively decompose both the capping molecules and the organic additives,[19,20] which part of this process is different from the impurity-free deposition technique. The air annealing process can transform the CuSe phase into undesired secondary phases before triggering liquid-phase sintering, which is determined by the thermal/chemical stability of the CuSe phase at elevated temperatures in air. It is well-known that the chalcogenide compounds are easily decomposable in the form of oxide phases at elevated temperatures in air. Thus, to adjust the microstructural evolution in CuSe-phase incorporating nanoparticle-based absorber layers, the thermal behavior of the CuSe phase in particulate films should be monitored. However, to date, the meaningful study on the thermally driven evolution of CuSe phase, in conjunction with consideration on the burn-out annealing of organic components, has been not reported, due to the lack of model material system for CuSe-phase incorporating nanoparticle-based absorber layer.

In this study, we report, for the first time, the thermal evolution of the CuSe phase in nanoparticle-based absorber layers, with a sophisticatedly controlled multiphase nanoparticles including CuSe phase that facilitate the formation of highly efficient, 8.2% solution-processed CISe photovoltaic devices.[6] The phase stability of the CuSe phase, associated with the formation of secondary phases during thermal treatment either in air or under inert atmosphere, is analyzed through a comparative investigation of both CuSe-phase including and CuSe-phase free nanoparticles. In addition, through in-depth investigation on CuSe-phase incorporating absorber layers, a thermal requisite is suggested for the preservation of the CuSe phase as well as for the complete decomposition of organic components.

2. EXPERIMENTAL SECTION

2.1. Raw Materials. All reagents for metal source, copper(II) acetate monohydrate ($Cu(CO_2CH_3)_2{\cdot}H_2O$, 98+ %,), indium(III) acetate ($In(C_2H_3O_2)_3$, 99.99%), and selenium powder (Se, 99.99%) were purchased from Aldrich and used as received without further purification. Ethylene glycol (EG, Aldrich, $HOCH_2CH_2OH$, 98%) and polyethylene glycol 400 (PEG 400, Junsei, $H[OCH_2CH_2]_nOH$, M_w = 400, extra pure) were used as solvents. Polyvinylpyrrolidone (PVP, Aldrich, $(C_6H_9NO)_n$, M_w = 55,000) was incorporated as an organic additive in preparing the CISe nanoparticle ink.

2.2. Synthesis of Multiphase (CuSe-Phase Including) and Single-Phase (CuSe-Phase Free) CISe Nanoparticles. For microwave-assisted synthesis of multiphase CISe nanoparticles, 0.6 g (2.9 mmol) of copper(II) acetate monohydrate, 1.43 g (4.9 mmol) of indium(III) acetate, and 0.75 g (9.8 mmol) of selenium powder were dissolved in 20 g of polyethylene glycol 400. In the case of multiphase nanoparticles, the indium is partially lost during annealing under Se atmosphere;[6] thus, the excess indium acetate was added in a reaction batch in order to reach the appropriate Cu/In ratio of ∼0.8. For microwave-assisted synthesis of single-phase CISe nanoparticles, 0.8 g (4.0 mmol) of copper(II) acetate monohydrate, 1.43 g (4.9 mmol) of indium(III) acetate, and 0.75 g (9.8 mmol) of selenium powder were dissolved in 20 g of ethylene glycol. In our synthetic pathway based on a microwave irradiation, the crystalline phases were predominantly determined by the chemical role of polyol solvents; the use of polyethylene glycol 400, with a long hydrocarbon chain between two hydroxyl groups facilitates the formation of multiphase CISe nanoparticles, while the ethylene glycol-based microwave synthesis results in a single phase CISe nanoparticls.[21] After stirring for 1 h at room temperature, each precursor solution was transferred to a Teflon liner vessel and heated under MW irradiation at 280 °C for 25 min. Upon completion of the synthesis reaction, the reaction solution was cooled to room temperature, and the nanoparticles were separated by centrifugation, collected, and washed three times with ethyl alcohol. Then, the resulting nanoparticles were dried under vacuum overnight at 40 °C to yield black powders. In order to investigate the crystalline structural evolution depending on annealing temperature and atmosphere, either multiphase or single-phase CISe nanoparticle was annealed at various temperatures between 200 and 530 °C for 30 min under Ar atmosphere or in air.

2.3. Ink Preparation and Film Formation. For the preparation of the colloidal functional ink, each nanoparticle was added with a solid content of 20 wt % in a mixed solvent with 0.72 g of ethyl alcohol and 1.68 g of ethylene glycol. Then, polyvinylpyrrolidone was added to the mixture of CISe nanoparticles and solvents, to form a crack-free layer. The prepared ink was mixed by ball milling to break the softly agglomerated nanoparticles and was subsequently deposited on a Mo/glass substrate. The resulting thin-film was dried at 80 °C in a vacuum oven. Selenization (annealing under Se atmosphere) was carried out in a vacuum evaporator equipped with a Knudsen-type effusion cell. The chamber was evacuated to a base pressure of 5×10^{-6} Torr, and the elemental Se was evaporated. The flux of Se vapor was adjusted by the effusion cell temperature and Se was effused at 180 °C. The samples were selenized at 300, 400, and 530 °C for 30 min on a hot plate located in the chamber.

2.4. Measurements. The compositional changes and the phase variations of multiphase and single-phase CISe nanoparticles depending on the annealing temperature and atmosphere were investigated using an energy dispersive spectrometer (EDS, Quantax 200, Bruker) and X-ray diffraction (XRD, D/Max 2200 V/PC, Rigaku), respectively. Selenized multiphase CISe films, including an organic additive, polyvinylpyrrolidone, were observed using a field emission scanning electron microscopy (FE-SEM, JSM-6700F, JEOL). The thermal behavior of the organic additive, polyvinylpyrrolidone, was monitored using a thermal gravimetric analysis (SDT2960, TA Instruments).

3. RESULTS AND DISCUSSION

3.1. The Temperature-Dependent Compositional and Crystalline Structural Evolution of Multiphase CISe Nanoparticles. The multiphase CISe nanoparticles synthesized in this study consisted of the chalcopyrite CISe phase, indexed to (112), (220), and (312), together with CuSe, $Cu_{2-x}Se$, and In_2O_3 secondary phases (Figure 1). In a previous

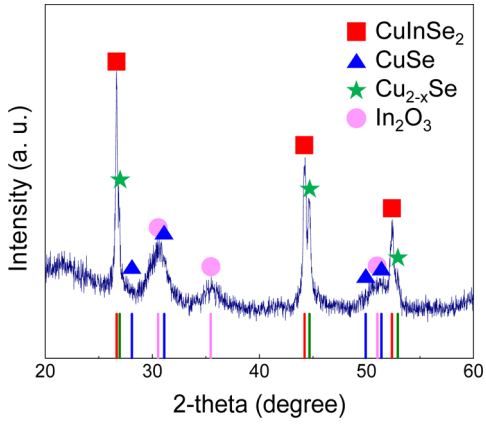

Figure 1. XRD spectrum for as-synthesized multiphase (CuSe phase-including) CISe nanoparticles.

study, the presence of the CuSe phase was proven with TEM-EDS composiitonal profile analysis on multiphase CISe nanoparticles.[21] Figure 2 shows both compositional and crystalline structural evolution, measured by EDS and XRD analysis, depending on the annealing temperature in air. The synthesized multiphase nanoparticles are spherical in shape and their average size is measured as ~80 nm (Figure S1). In the

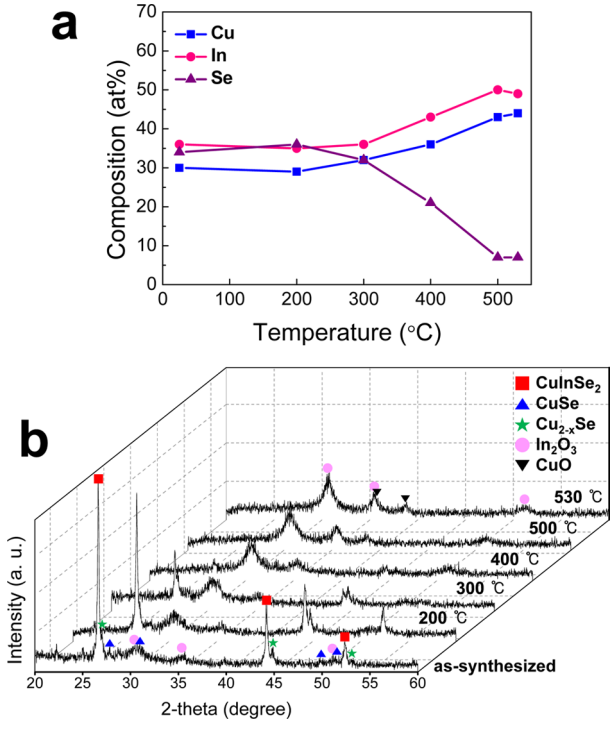

Figure 2. (a) Compositional (atomic ratio) variation and (b) XRD spectra for as-synthesized multiphase (CuSe phase-including) CISe nanoparticles annealed at 200, 300, 400, 500, and 530 °C in air.

case metal nanoparticles, the thermal properties including a melting behavior is predominantly influenced by a particle size; the CI(G)S chalcogenide nanoparticles, however, do not undergo such a characteristic thermal behavior as a function of nanoparticle size. It was reported that the CIGS nanoparticles, even with the particle below 10 nm, do not melt by a high temperature annealing above 500 °C, maintaining the individual particle morphology, crystalline structure, and composition.[19] Therefore, in investigating the thermal evolution of multiphase nanoparticles, the particle size effect was not taken into consideration. As can be seen in Figure 2a, the Se content decreased gradually above 200 °C, while the Cu content increased together with the In content. There are three plausible reasons for these phenomena: (i) the decomposition reaction of the CuSe phase into the $Cu_{2-x}Se$ phase, leading to the evaporation of the low melting point Se phase,[7,9,12,22−24] (ii) the oxidation of CISe, CuSe, and $Cu_{2-x}Se$ phases into Cu_xO, In_2O_3, and SeO_2 phases, and (iii) the formation of In_xSe_y, which has a volatile nature. In particular, the formation of the volatile SeO_2 phase (T_m: 340 °C) can contribute dominantly to the Se loss.[6] However, the third reason can be excluded if we take into consideration the identical slopes in the compositional change of Cu and In. The proposed phase transitions, based on a compositional evolution, were also confirmed by the crystalline structural evolution at elevated temperatures in air (Figure 2b). The main CISe phase disappeared gradually between 200−400 °C, mainly above 300 °C, and oxide phases of In_2O_3 and CuO began to form above 300 °C. The additional formation of the $Cu_{2-x}Se$ phase, by decomposition of the CuSe phase, was not observed. Theoretically, the phase transition of CuSe into the $Cu_{2-x}Se$ phase is favorable thermodynamically above 380 °C in an oxygen-free atmosphere. However, since the formation of oxide phases from Cu−Se compounds proceeded at lower temperatures, the contribution of the CuSe-$Cu_{2-x}Se$ phase transition is believed not to be predominant. Therefore, it is speculated that the compositional variation of Cu, In, and Se is caused by the formation of Cu_xO, In_2O_3, and volatile SeO_2 oxide phases from CISe, CuSe, and $Cu_{2-x}Se$ phases.

In contrast, no noticeable changes in composition and crystalline structure were seen under inert atmosphere even at high temperatures (Figure 3). The formation of oxide phases is restricted because of the lack of oxidants under the oxygen-free atmosphere. The phase transition between Cu−Se compounds was not activated vigorously enough to be detectable by rough EDS and XRD analysis, since the transformation from the CuSe phase to the $Cu_{2-x}Se$ phase is suppressed by the structurally impedimental interaction with the main CISe phase.[9,22,23] Only the thermally enhanced crystallization of the main CISe phase was observed, as a thermal behavior of multiphase nanoparticles under inert atmosphere. This temperature independency of Cu, In, and Se composition under oxygen-free atmosphere reflects the facile processability in optimizing the annealing process, without the consideration on compositional variation. For Cu−In−(Ga)−Se nanoparticle systems, the binary chalcogenide and chalcopyrite phases are commonly unstable at elevated temperatures, even under oxygen-free atmosphere, owing to the presence of environmentally vulnerable, energetically unstable surface atoms; this situation brings an impediment in adjusting the annealing process for the generation of high-performance chalcopyrite thin-films. It has been reported that the decomposition of CI(G)Se nanoparticles occurs in the form of In_2Se (g) and Ga_2Se (g), even under N_2 atmosphere, when the temperature approaches 500 °C for inducing micro-

dx.doi.org/10.1021/am401735a | ACS Appl. Mater. Interfaces 2013, 5, 6930−6936

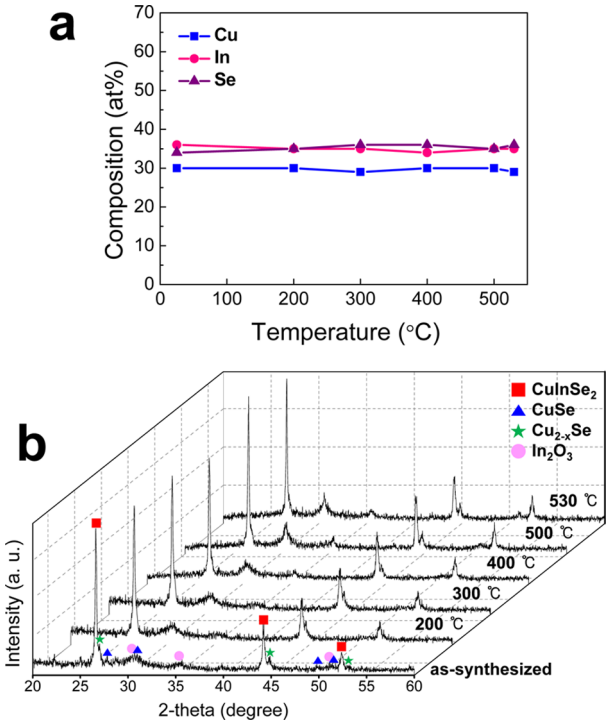

Figure 3. (a) Compositional (atomic ratio) variation and (b) XRD spectra for as-synthesized multiphase (CuSe phase-including) CISe nanoparticles annealed at 200, 300, 400, 500, and 530 °C under nitrogen atmosphere.

structural densification.[25] The characteristic phase-stability of the multiphase nanoparticles, synthesized in this study, is attributed to the strong chemical binding of surface atoms by polyol molecules, which prevents chemical interaction with other moieties forming the volatile phases. In wet-chemical synthesis using polyol solvents, the polyol molecule surrounds effectively the nanoparticle surface through a covalent bonding with metal cations prior to a nanoparticle nucleation.

3.2. The Temperature-Dependent Compositional and Crystalline Structural Evolution of Single-Phase CISe Nanoparticles. For single-phase CISe nanoparticles, the compositional change and phase evolution at elevated temperatures were analyzed further in order to figure out which phase transition is predominantly involved with the CuSe phase and how those transition reactions can be suppressed or activated. The major diffraction peaks of the single-phase CISe nanoparticles are indexed to (112), (220), and (312), as a pure chalcopyrite phase (Figure 4). The In_2O_3 phase appeared to be present together with the CISe phase, but its intensity is negligible, indicating the presence in an extremely small amount. The size synthesized single-phase nanoparticles were measured as ~95 nm (Figure S1), which is almost corresponding to that of multiphase nanoparticles. Figure 5 shows the compositional variation and crystalline structural evolution of the single-phase CISe nanoparticles during annealing under inert atmosphere. Cu, In, and Se contents in the films were found to be independent of the annealing temperature. Phase transitions in single-phase CISe thin-films did not take place during annealing up to 530 °C; this annealing was accompanied only by enhanced crystallinity above 500 °C. Such thermal behavior, which shows no noticeable variation depending on annealing temperature, is identical to that of multiphase CISe nanoparticles, indicating

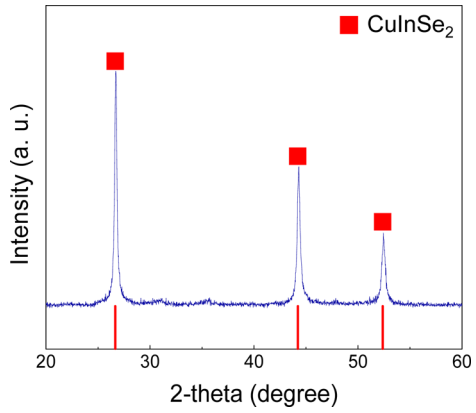

Figure 4. XRD spectrum for as-synthesized single-phase (CuSe-phase free) CISe nanoparticles.

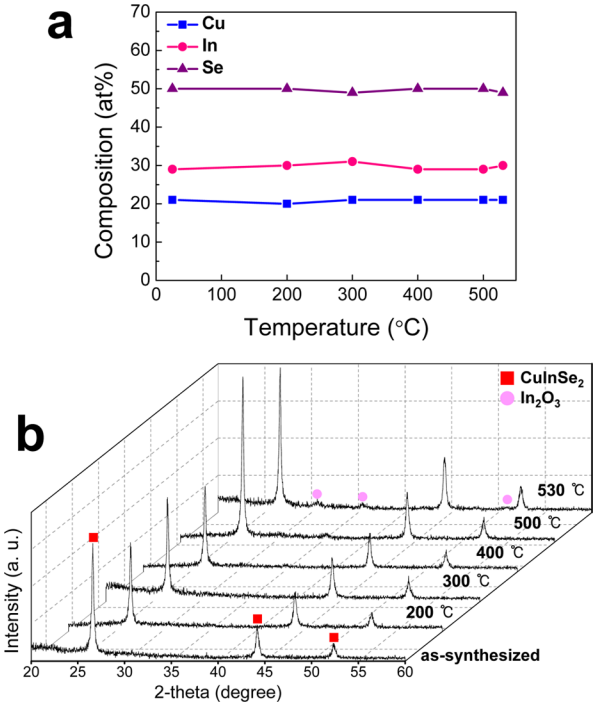

Figure 5. (a) Compositional (atomic ratio) variation and (b) XRD spectra for as-synthesized single-phase (CuSe-phase free) CISe nanoparticles annealed at 200, 300, 400, 500, and 530 °C under nitrogen atmosphere.

that the polyol molecules, both of PEG 400 and EG, play a role in stabilizing the nanoparticle surface atoms. However, in the case of annealing in air, evidently different compositional and crystalline structural evolutions were observed. In the compositional analysis (Figure 6a), the single-phase CISe nanoparticles were found to be stable up to 300 °C, showing no change in composition. From the XRD analysis (Figure 6b), it can be observed that the oxide phases evolved above 300 °C and the oxidized phases started being crystallized further above 300 °C. Therefore, based on all of the analyses of the thermal behavior in air for both multiphase and single-phase CISe nanoparticles, it can be revealed that the oxidation of secondary phases, including the CuSe phase, occurs predominantly between 200 and 300 °C, while the oxidation of the main CISe phase takes place above 300 °C. Thus, if a primary heat-treatment in air is required, it should be carried out below 200 °C in order to

dx.doi.org/10.1021/am401735a | ACS Appl. Mater. Interfaces 2013, 5, 6930−6936

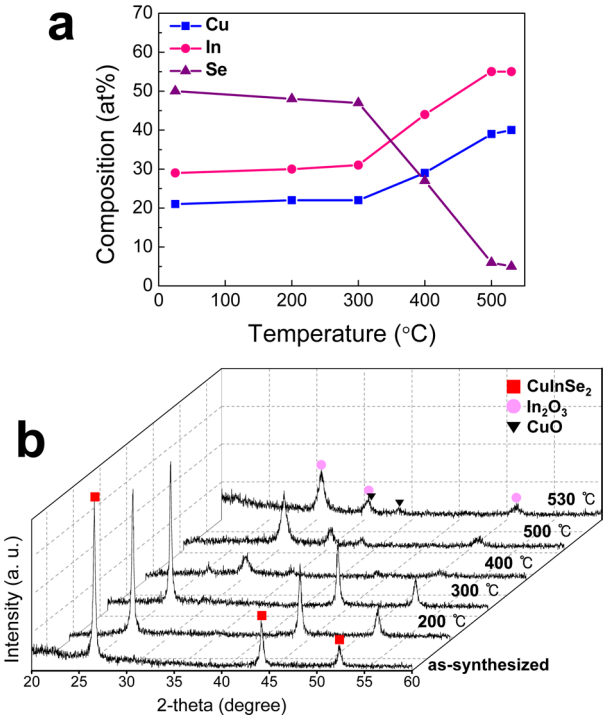

Figure 6. (a) Compositional (atomic ratio) variation and (b) XRD spectra for as-synthesized single-phase (CuSe-phase free) CISe nanoparticles annealed at 200, 300, 400, 500, and 530 °C in air.

prevent the formation of undesirable phases from the CuSe phase. This indicates that the decomposition of the organic components, which are inevitably incorporated for the formation of crack-free thin-films or the preparation of functional inks with adequate rheological properties, should be complete below 200 °C in air; thus, the selection of organic additives that can be thermally decomposed below 200 °C in air is a principal prerequisite in attempts to generate high-performance solution-processed chalcopyrite thin-films from CuSe-phase including nanoparticles. However, organic additives that comply with this thermal decomposition behavior are rarely present due to the basic chemical nature of organic compounds. Alternatively, organic additives that are thermally decomposable even at high temperature under inert atmosphere can be incorporated, since the phases are preserved well under oxygen-free atmosphere at elevated temperatures. However, from the viewpoint of microstructural evolution, the thermal decomposition should be complete below a certain temperature at which the microstructural densification takes place, which will be described in a later section. In addition, under oxygen-free atmosphere, the supply of sufficient Se vapor is required during heat treatment for restricting the decomposition of CuSe to $Cu_{2-x}Se$ as well as inducing a phase transition of oxides into chalcogenides.

3.3. The Temperature-Dependent Compositional and Crystalline Structural Evolution of Multiphase CISe Thin-Films Including Organic Components under Se Atmosphere. The compositional and crystalline structural variation was shown in Figure 7 for multiphase CISe thin films deposited with an organic additive, PVP. The CISe films, derived from PVP-free CISe nanoparticle ink, suffer from micrometer-sized cracks; this flaw has a critical adverse influence on the establishment of an acceptable heterogeneous junction between the CdS and absorber layer.[6] As can be seen in Figure 7a, no noticeable compositional variations were observed below 300 °C. Above 400 °C, Se composition increased due to Se substitution for oxygen in In_2O_3; also, the Cu/In ratio was adjusted to 0.8 by the formation of the volatile In−Se phase.[6] In terms of the crystalline structural evolution (Figure 7b), at 400 °C, the phase transition to CISe phase proceeded slightly. The ratio of the peak at 26.7° (CISe) to the peak at 31.1° (CuSe) increased from 1.2 to 1.3, when the selenization temperature increased from 300 to 400 °C. This restricted crystalline structural evolution is associated with the interference of PVP for the phase transformation. The thermal decomposition of PVP starts at 340 °C and is completed at 450 °C under an oxygen-free atmosphere (Figure S2). As can be seen in Figure S3, for the PVP-free multiphase CISe particulate layer, the ratio of the peak at 26.7° (CISe) to the peak at 31.1° (CuSe) was 7.75 upon selenization at 400 °C, indicative of the negative impact of the organic additives on phase transformations. In addition, after selenization at 400 °C, a very thin dense layer with a thickness of 180 nm was formed on the surface layer (Figure 8a). It is presumed that the formation of thin dense layer results from the partial solid-state densification by the CuSe phase, prior to the liquid phase formation. The solid-state densification is, in general, triggered at around $0.7xT_m$ (melting point) for a certain phase, and the melting point of the CuSe phase is 523 °C. When the annealing temperature reached 530 °C, the transformation into single CISe phase was completed and no secondary phases were observed, yielding a pore-free and well-crystallized CISe layer (Figure 8b). When a liquid phase forms via melting of CuSe, the solid dissolves and diffuses through the liquid; the solid

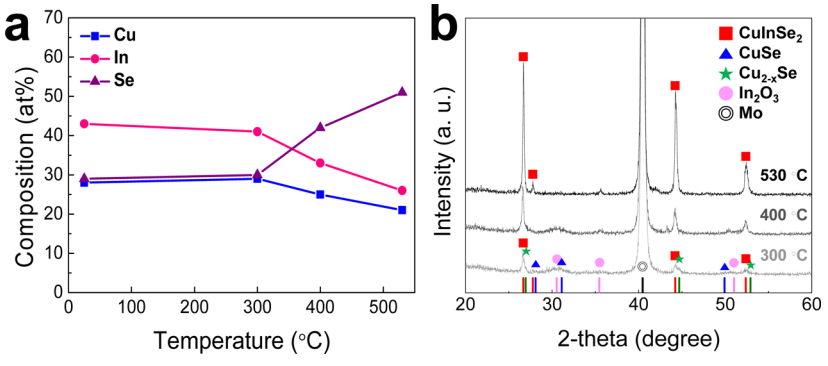

Figure 7. (a) Compositional (atomic ratio) variation and (b) XRD spectra for multiphase (CuSe phase-including) CISe films, with an organic additive, PVP, depending on the selenization temperature.

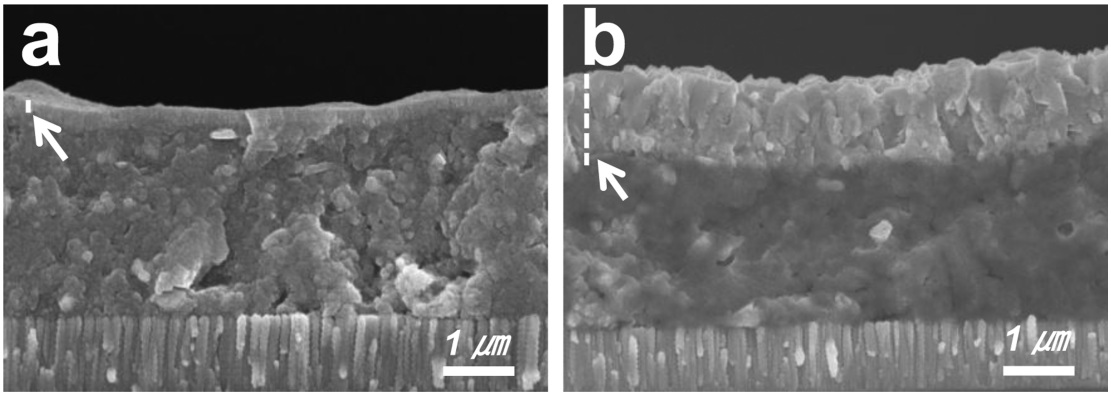

Figure 8. SEM images for multiphase (CuSe phase-including) CISe films, including an organic additive, PVP, selenized at (a) 400 and (b) 530 °C. The dashed line and arrow indicate the upper, dense CISe layer.

then precipitates on the particles at other sites, resulting in densification of the solid particulate network. However, it is observed that the resulting CISe layer is composed of a bilayer structure: a dense, well-crystallized layer with a thickness of 1.3 μm as the upper layer and an amorphous layer as the lower layer. As the dense CISe layer forms from the surface of the multiphase particulate layer, organic moieties, which result from the complete thermal decomposition of the organic additive, are not evaporated through the preformed dense CISe layer; these moieties remain with the completely transformed CISe component. This organic-residue remaining in the bilayer structure results in a high series resistance (R_s) and/or high shunt conductance (G_{sh}) in the overall device structure, both of which have a critical impact on device performance.[20,26,27] In this regard, for creating the device-quality absorber layer using the CuSe-phase incorporating nanoparticle-based approach, the annihilation of organic residues should be performed with a thermal treatment through which the CuSe phase is not decomposed and the solid-state/liquid phase densification is triggered. Therefore, for achieving high performance, nanoparticle-based chalcopyrite absorber layers through an effective liquid-phase densification induced by the CuSe phase, an in-depth consideration should be taken in terms of the strategy for incorporating organic additives that can be easily decomposable via thermal treatment below 200 °C in air or that can be evaporated prior to triggering the solid-state densification by the CuSe phase in an oxygen-free atmosphere.

4. CONCLUSION

In summary, the compositional and crystal structural stability of the CuSe phase, incorporated as a crucial phase for inducing liquid-phase densification, were investigated based on a comparative analysis with CuSe phase-including and CuSe phase-free nanoparticles. It was revealed that the CuSe phase incorporated in the nanoparticle system was stable even at high temperatures above 500 °C under inert atmosphere; on the other hand, this CuSe phase was decomposable above 200 °C in air owing to the oxidation reaction. In addition to these criteria for the thermal stability of CuSe-phase including nanoparticles, it was also demonstrated that the thermal decomposition behavior of organic additives plays a critical role in determining the microstructural evolution of the CuSe-phase including nanoparticle-based chalcopyrite films and that the decomposition of the organic additives should be completed prior to triggering the solid-state densification by the CuSe phase.

■ ASSOCIATED CONTENT

Supporting Information

SEM images for single-phase and multiphase CISe nanoparticles, TGA result for PVP under N_2 atmosphere, and XRD result for the CISe layer prepared from the PVP-free CISe ink. This material is available free of charge via the Internet at http://pubs.acs.org.

■ AUTHOR INFORMATION

Corresponding Author

*E-mail: sjeong@krict.re.kr.

Notes

The authors declare no competing financial interest.

■ ACKNOWLEDGMENTS

This study was supported by a grant from the cooperative R&D program funded by the Korea Research Council of Industrial Science and Technology and was partially supported by the Industrial Core Technology Development Program, funded by the Ministry of Knowledge Economy (No. 10031709, Development of Direct Nanopatterning Technology for Electronic Devices). This work was also supported by a National Research Foundation of Korea (NRF) grant funded by the Korea government (MEST) (No. 2012R1A3A2026417).

■ REFERENCES

(1) Yang, Y.-H.; Chen, Y.-T. *J. Phys. Chem. B* **2006**, *110*, 17370−17374.
(2) Acciarri, M.; Donne, A. L.; Morgano, M.; Caccamo, L.; Miglio, L.; Marchionna, S.; Moneta, R.; Meschia, M.; Binetti, S. *Energy Procedia* **2011**, *10*, 138−143.
(3) Wu, Y.; Wadia, C.; Ma, W.; Sadtler, B.; Alivisatos, A. P. *Nano Lett.* **2008**, *8*, 2551−2555.
(4) Guo, Q.; Ford, G. M.; Hillhouse, H. W.; Agrawal, R. *Nano Lett.* **2009**, *9*, 3060−3065.
(5) Guo, Q.; Ford, G. M.; Agrawal, R.; Hillhouse, H. W. *Prog. Photovoltaics* **2013**, *21*, 64−71.
(6) Jeong, S.; Lee, B.-S.; Ahn, S. J.; Yoon, K. H.; Seo, Y.-H.; Choi, Y.; Ryu, B.-H. *Energy Environ. Sci.* **2012**, *5*, 7539−7542.
(7) Yoon, S.; Yoon, T.; Lee, K.-S.; Yoon, S.; Ha, J.; Choe, S. *Sol. Energy Mater. Sol. Cells* **2009**, *93*, 783−788.
(8) Chowlesa, A. G.; Engelbrechtb, J. A. A.; Neethlingb, J. H.; Theronc, C. C. *Thin Solid Films* **2000**, *361−362*, 93−97.
(9) Wolf, D.; Mueller, G. *Thin Solid Films* **2000**, *361−362*, 155−160.
(10) Moon, D. G.; Ahn, S. J.; Yun, J.; Cho, A.; Gwak, J.; Ahn, S.; Shin, K.; Yoon, K. H.; Lee, H.-D.; Pak, H.; Kwon, S. *Sol. Energy Mater. Sol. Cells* **2011**, *95*, 2786−2794.

(11) Volobujeva, O.; Altosaar, M.; Raudoja, J.; Mellikov, E.; Grossberg, M.; Kaupmees, L.; Barvinschi, P. *Sol. Energy Mater. Sol. Cells* **2009**, *93*, 11−14.
(12) Lakshmi, M.; Bindu, K.; Bini, S.; Vijayakumar, K. P.; Kartha, C. S.; Abe, T.; Kashiwaba, Y. *Thin Solid Films* **2001**, *386*, 127−132.
(13) Pai, R. R.; John, T. T.; Lakshmi, M.; Vijayakumar, K. P.; Kartha, C. S. *Thin Solid Films* **2005**, *473*, 208−212.
(14) Vernals, S.; Orbey, N.; Birkmire, R. W.; Russell, T. W. F. *Prog. Photovoltaics* **1996**, *4*, 341−353.
(15) Vinod, T. P.; Jin, X.; Kim, J. *Mater. Res. Bull.* **2011**, *46*, 340−344.
(16) Zhang, A.; Ma, Q.; Wang, Z.; Lu, M.; Yang, P.; Zhou, G. *Mater. Chem. Phys.* **2010**, *124*, 916−921.
(17) Zainal, Z.; Nagalingam, S.; Loo, T. C. *Mater. Lett.* **2005**, *59*, 1391−1394.
(18) Xu, S.; Wang, H.; Zhu, J.-J.; Chen, H.-Y. *J. Cryst. Growth* **2002**, *234*, 263−266.
(19) Panthani, M. G.; Akhavan, V.; Goodfellow, B.; Schmidtke, J. P.; Dunn, L.; Dodabalapur, A.; Barbara, P. F.; Korgel, B. A. *J. Am. Chem. Soc.* **2008**, *130*, 16770−16777.
(20) Ahn, S. J.; Kim, K.; Cho, A.; Gwak, J.; Yun, J. H.; Shin, K.; Ahn, S. K.; Yoon, K. H. *ACS Appl. Mater. Interfaces* **2012**, *4*, 1530−1536.
(21) Seo, Y.-H.; Lee, B.-S.; Jo, Y.; Kim, H.-G.; Choi, Y.; Ahn, S. J.; Yoon, K. H.; Woo, K.; Moon, J.; Ryu, B.-H.; Jeong, S. *J. Phys. Chem. C* **2013**, *117*, 9529−9536.
(22) Wolf, D.; Muller, G. *Mater. Res. Soc. Symp. Proc.* **1997**, *485*, 173.
(23) Wolf, D.; Muller, G.; Stetter, W.; Karg, F. *Proceedings of the 2nd World Conference on Photovoltaic Solar Energy Conversion, Vienna, Austria* **1998**, 2426−2430.
(24) Stolen, S.; Fjellag, H.; Gronvold, F.; Sipowska, J. T.; Westrum, E. F. *J. Chem. Thermodyn.* **1996**, *28*, 753−766.
(25) Ahn, S. J.; Kim, C. W.; Yun, J. H.; Lee, J. C.; Yoon, K. H. *Sol. Energy Mater. Sol. Cells* **2007**, *91*, 1836−1841.
(26) Ahn, S. J.; Kim, C. W.; Yun, J. H.; Gwak, J.; Jeong, S.; Ryu, B.-H.; Yoon, K. H. *J. Phys. Chem. C* **2010**, *114*, 8108−8113.
(27) Kim, K.; Eo, Y.-J.; Cho, A.; Gwak, J.; Yun, J. H.; Shin, K.; Ahn, S. K.; Park, S. H.; Yoon, K.; Ahn, S. J. *J. Mater. Chem.* **2012**, *22*, 8444−8448.